THE ARCHIVE OF MECHANICAL ENGINEERING

VOL. LIII 2006 Number 3

Key words: *wind turbine, wind turbine aerodynamics*

PIOTR STRZELCZYK *

THE METHOD OF CALCULATION OF HORIZONTAL AXIS WIND TURBINE PERFORMANCE AT YAWED FLOW CONDITIONS BY THE USE OF SIMPLIFIED VORTEX METHOD

In the paper, the author presents a certain method of calculation of Horizontal Axis Wind Turbine (HAWT) performance for yawed flow conditions. The presented model is developed on the basis of propeller theory described in [23]. Te model employs the results of the vortex theory of propeller combined with momentum and angular momentum theorems for the HAWT wake. In the model, the blade element is regarded as a source of tangential and axial force acting on air at actuator disk surface. The momentum equations are corrected for the effect of finite number of blades by introduction of Prandtl tip-loss factor to the equations. Thanks to the approximation of lift force coefficient vs. angle of attack by sine curve, one may get a quadratic equation for local axial velocity component. Tangential component of induced velocity may be calculated from relations obtained from vortex theory of HAWT. This allows us to avoid an iterative solution for induced velocity, unlike in most of the HAWT and propeller theories. The blade section drag is incorporated to calculations of total drag of rotor and power, when induced velocity components are known, and hence blade element angle of attack is determined. To incorporate the effect of blade element stall-delay due to blade rotation, a simple semi-empirical model proposed by Tangler and Selig has been applied. The calculations are compared with experimental data obtained at Risϕ 100 kW experimental turbine test site and at the Grumman Wind Stream 33 turbine modified by NREL. The comparison includes power output as well as blade element angles of attack. The presented results show that the method described in the paper underestimates performance for low speed winds, whereas for strong winds the power output is slightly overestimated. For average angles of attack, one may see that for small tip speed ratios angles of attack are overestimated. At high tip speed ratios, however, angles of attack are underestimated. It was shown that there is a need to take into account the work done by side force on the tangential inflow component to obtain correct power curves for yawed flow conditions.

* *Rzeszów University of Technology Faculty of Mechanical Engineering and Aeronautics, ul. Wincentego Pola 2, 35-959 Rzeszów, Poland; E-mail: piotstrz@prz.edu.pl*

NOMENCLATURE

A	blade shape parameter,	–
a_0	lift curve slope at zero lift angle of attack,	1/rd
B	number of blades,	–
c	chord of blade,	m
C_L	lift coefficient,	–
C_D	drag coefficient,	–
$C_P = 2P/\pi\rho V_w^3 R^2$	power coefficient,	–
F	Prandtl tip-loss factor,	–
F_x, F_y, F_z	components of rotor forces (see: fig. 1),	N
H	hub height,	m
M	rotor torque,	Nm
P	power,	W
R	rotor tip radius,	m
r	local radius,	m
V_N	component of wind speed normal to the rotor plane,	m/s
V_T	peripheral component of wind speed,	m/s
$V_W(H)$	wind speed at hub height,	m/s
$\tilde{V}_W = V_W(z_g)/V_W(H)$	dimensionless wind speed,	–
V_X	axial component of velocity at rotor plane,	m/s
V_θ	tangential (swirl) component of induced velocity,	m/s
W	Resultant inflow velocity at blade element,	m/s
x, y, z	Cartesian coordinates referred to the rotor disk,	m
x_g, y_g, z_g	Cartesian coordinates referred to the ground,	m
Greek letters:		
α	blade-section angle of attack,	rd
α_0	blade-section zero-lift angle of attack,	rd
α_r	rotor tilt angle,	rd
$\alpha^{(0)} = \alpha - \alpha_0$	blade-section aerodynamic angle of attack,	rd

β	local blade setting angle,	rd
$\beta^{(0)} = \beta - \alpha_0$	aerodynamic blade setting angle,	rd
Γ	blade-section circulation,	m^2/s
Γ_∞	circulation for infinite number of blades,	m^2/s
$\lambda = \omega R/V_\infty$	tip speed ratio,	–
$\xi = r/R$	dimensionless radial coordinate,	–
ξ_0	dimensionless hub radius,	–
ρ	air density,	kg/m^3
$\sigma = Bc/2\pi r \equiv B\bar{c}/2\pi\xi$	local solidity of rotor,	–
ϕ	local inflow angle,	rd
$\chi_p = C_L/a_0 \sin\alpha^{(0)}$	blade-element "efficiency",	–
ψ	blade azimuth angle,	rd
ω	angular velocity of turbine axis.	rd/s

1. Introduction

The proper determination of the aerodynamic characteristics of wind turbine is very important due to prediction of production of energy by the wind energy power plant. Therefore, many models of the wind turbine aerodynamic have been developed. Some of the models match blade element theory and momentum theorem [14], [16], [18], [21], [24], [29], with correction for finite number of blades [8]. Other methods employ the lifting line theory of propeller [1], [15], [17], lifting surface methods based on vortex lattice[2], [27], [28], acceleration potential methods [5], [6] or panel methods [4]. Some authors developed HAWT models matching blade element method and actuator disk theory with viscous flow in the wake taken into account [19]. However, real wind turbine is working under complex, non-uniform wind conditions caused by mean vertical velocity profile, twist of wind direction, rapid changes of wind direction, atmospheric turbulence, and blade flapping. In the case of windward placed rotors, the tower shadow must be taken into account [7], [10], [12], [27]. Yawed inflow may be also caused by an error of wind turbine control system (due to wind flag[1] placed in the flow disturbed by rotor and nacelle). The yaw of the rotor is sometimes applied as a method of control, especially for small turbines. Hence, the HAWT working in non-symmetrical is of interest of aerodynamicists and industry [4], [5], [10], [12], [13], [26], [27], [28].

[1] Wind direction indictor, which generates a signal for yaw channel of turbine control system.

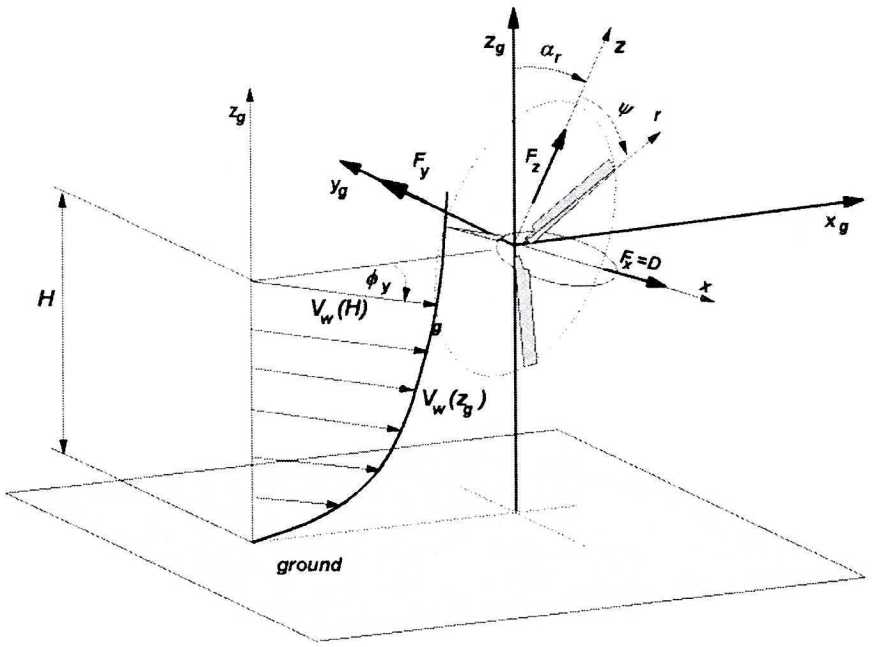

Fig. 1. HAWT at non-uniform, yawed flow

The method of determination of HAWT performance in non-uniform flow may be regarded as a generalization of the method of calculation of HAWT performance proposed by the author in [21], and [22] and may be treated as a counterpart of the method of analysis of propeller at angle of incidence [22]. The presented model couples a local momentum and angular momentum theorem with lifting line model based on Prandtl tip loss factor. In the paper [9], Hall has introduced tip loss coefficient for skewed propeller wake; approximation of lift curve by sinusoid [21], [22], [23], [29] allows us to obtain an analytical solution both for axial and tangential components of induced velocity for given radius and azimuth of the blade. There is no need to make any additional assumptions on values of induced velocities like in [3], [12], [13]. In the paper, we will show a necessity for correction of the power curve for an additional power dependent on work done at unit time by tangential force acting in rotor plane.

2. Basic equations of the model

The model of HAWT rotor flow applied in the present paper is based on the following assumptions: In the present section, the following assumptions are made:

1. The profile drag is neglected in the flow analysis;

2. The swirl component of the average velocity increases from zero just in front of actuator disc to its full value in the far wake;
3. The velocity induced by bound vortices can be neglected[2];
4. The pressure in he far wake is equal to the ambient pressure;
5. Blades are infinitely rigid, so flapping motions and blade torsion could be neglected.
6. The inflow non-uniformity is caused by:
   6a. vertical profile of the velocity;
   6b. yaw angle of the rotor;
   6c. rotor tilt angle;

The scheme of the inflow conditions on the HAWT actuator disk is presented in Fig. 1. The circulation of the velocity around a single blade of the B-blade rotor is coupled with circulation of averaged velocity field by Prandtl tip loss factor F [8]:

$$F := \frac{B\Gamma}{\Gamma_\infty} \tag{1}$$

where: Γ_∞ – circulation for infinite number of blades; B-number of blades; Γ – circulation around the single blade. The value of the tip-loss factor is given by formula:

$$F = \frac{2}{\pi}\arccos\left(\exp\left(\frac{B}{2}\frac{\xi - 1}{\sin\phi_T}\right)\right) \tag{2}$$

The circulation for single blade is equal:

$$\Gamma = \frac{1}{2}WcC_L \tag{3}$$

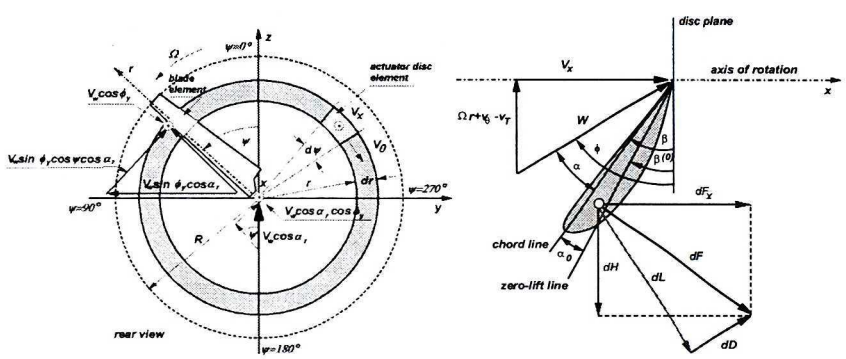

Fig. 2. Flow through the actuator disk and forces acting at the blade element. Schematic

[2] Justification of this assumption for the straight blades one may find in [3] at p. 126.

Making use of the above assumptions and formulae (1) and (3), one can express elementary torque and axial force in the following form:

$$\frac{d^2M_{id}}{drd\psi} \equiv \frac{1}{4\pi}\rho W^2 BcC_L \sin\phi r dr d\psi = \rho 2V_\theta V_X r^2 F dr d\psi \tag{4}$$

$$\frac{d^2F_{xid}}{drd\psi} \equiv \frac{1}{4\pi}\rho W^2 BcC_L \cos\phi dr d\psi = 2V_X (V_N - V_X) rF dr d\psi \tag{5}$$

Where normal and tangential components of wind speed at the element of actuator disk are equal:

$$V_N = V_w \cos\alpha_r \cos\phi_y \tag{6}$$

$$V_T = V_w \left(\sin\alpha_r \sin\psi - \cos\alpha_r \sin\phi_y\right) \tag{7}$$

the relative velocity W is equal:

$$W = \sqrt{(\omega r - V_T + V_\theta)^2 + V_X^2} \tag{8}$$

From Eqs. (4) and (5) one may obtain:

$$tg\phi = \frac{V_\theta}{V_N - V_X} \tag{9}$$

The second relationship for inflow angle may be obtained from velocity triangles shown in Fig. 2:

$$tg\phi = \frac{V_X}{\Omega r - V_T + V_\theta} \tag{10}$$

form (9) and (10) one may get the following relation:

$$V_X (V_N - V_X) = (\Omega r - V_T) V_\theta + V_\theta^2 \tag{11}$$

Because tangential component of induced velocity is small in comparison with blade element velocity Ωr and axial velocity V_x, equation (11) may be linearised by neglecting the second order small term V_θ^2 Hence, we obtain the following relationship between axial velocity at actuator disk element and the tangential induced velocity:

$$V_\theta = \frac{V_X (V_N - V_X)}{\Omega r - V_T} \tag{12}$$

or in non-dimensional form:

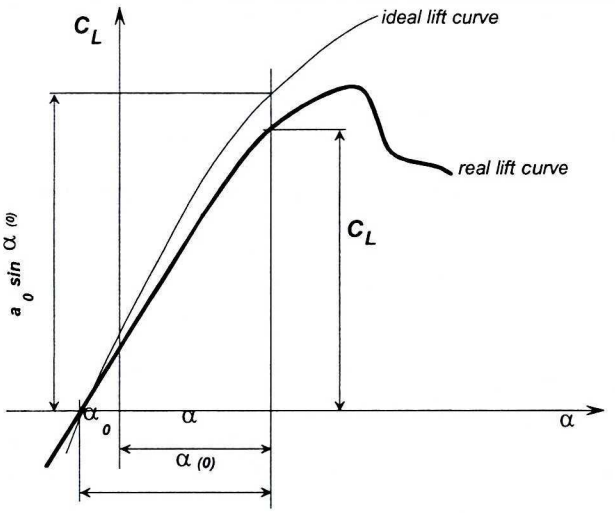

Fig. 3. The lift curve

$$\bar{V}_\theta = \frac{\bar{V}_X\left(\bar{V}_N - \bar{V}_X\right)}{\xi - \bar{V}_T} \tag{12a}$$

Making use of torque equation (4) and a velocity triangle in Fig. 2, one may obtain the following relation:

$$\bar{W}\sigma C_L = 4\bar{V}_\theta F \tag{13}$$

Following the work by Witoszyński [29], it is convenient to express lift coefficient curve in the following form [21], [23]:

$$C_L = a_0 \chi_p\left(\alpha^{(0)}, \mathrm{Re}, Ma\right)\sin\alpha^{(0)} \tag{14}$$

The representation of lift curve is depicted schematically in Fig. 3. The formula (14) represents an ideal lift curve corrected for the viscosity effects. The angle of attack measured from zero lift line is equal to:

$$\alpha^{(0)} = \phi - \beta^{(0)} \tag{15}$$

Inserting (14) and (15) into (13) and neglecting higher order term proportional to square of swirl velocity, one obtains quadratic equation for V_x. The solution of this equation is:

$$\bar{V}_x = \frac{A - \bar{V}_N}{2} + \sqrt{\left(\frac{A - \bar{V}_N}{2}\right)^2 + A\left(\xi - \bar{V}_T\right) tg\beta^{(0)}} \tag{16}$$

Where "blade element shape coefficient" A takes the form:

$$A = \frac{\sigma a_0 \chi_p}{4} \frac{\left(\xi - \bar{V}_T\right) \cos\beta^{(0)}}{F + \frac{\sigma a_0 \chi_p}{4} \sin\beta^{(0)}} \tag{17}$$

the local inflow angle may be calculated from the following formula:

$$\phi = arc\, tg \frac{\bar{V}_\vartheta}{2\left(\bar{V}_N - \bar{V}_x\right)} \tag{18}$$

From formulae (14) and (15) one may calculate the angle of attack and hence sectional lift and drag coefficients.

The axial force F_x side force F_y, F_z and torque M may be calculated from the analysis of forces acting on the blade element. The rotor axial force coefficient may be calculated from:

$$C_{F_x} = \frac{\lambda^2}{\pi} \int_0^{2\pi} \int_{\xi_h}^{1} \bar{W}^2 \sigma \left(C_L \cos\phi + C_D \sin\phi\right) \xi d\xi d\psi \tag{19}$$

Elemental components of side force are given by the formulae:

$$dF_y = -dH \cos\psi \tag{20}$$

$$dF_z = -dH \sin\psi \tag{21}$$

where elemental tangential force dH (Fig. 2) is:

$$dH = \frac{\rho W^2 B c}{2} \left(C_L \sin\phi - C_D \cos\phi\right) dr d\psi / 2\pi \tag{22}$$

Hence, the coefficients of side force are given by the following formulae:

$$C_{Fy} = -\frac{\lambda^2}{\pi} \int_0^{2\pi} \int_{\xi_0}^{1} \bar{W}^2 \sigma \left(C_L \sin\phi - C_D \cos\phi\right) \cos\psi \xi d\xi d\psi \tag{23}$$

$$C_{Fz} = -\frac{\lambda^2}{\pi} \int_0^{2\pi} \int_{\xi_0}^{1} \bar{W}^2 \sigma \left(C_L \sin\phi - C_D \cos\phi\right) \sin\psi \xi d\xi d\psi \tag{24}$$

The power extracted from wind by the yawed rotor must be divided into part dependent on torque, and the work done in unit time by the components of tangential force on the tangential components of inflow velocity. Two latter

parts of power absorbed from the wind by rotor are analogous to the part of profile power dependent on advance ratio for helicopter rotor in forward flight [11]. This case is also similar to that of propeller at angle of incidence [23]. Hence, the useful mechanical power is equal:

$$P = M\omega - P_y - P_z \tag{25}$$

The power coefficients related to the side force components are:

$$C_{Py} = \frac{\lambda^2 \cos\alpha_r \sin\phi_y}{\pi} \int_0^{2\pi} \int_{\xi_0}^{1} \tilde{V}_w \bar{W}^2 \sigma (C_L \sin\phi - C_D \cos\phi) \cos^2\psi \xi d\xi d\psi \tag{26}$$

$$C_{Pz} = \frac{\lambda^2 \sin\alpha_r}{\pi} \int_0^{2\pi} \int_{\xi_0}^{1} \tilde{V}_w \bar{W}^2 \sigma (C_L \sin\phi - C_D \cos\phi) \sin\psi \, \xi d\xi d\psi \tag{27}$$

and the component related to the torque is equal:

$$C_{PM} = \frac{\lambda^3}{\pi} \int_0^{2\pi} \int_{\xi_0}^{1} \bar{W}^2 \sigma (C_L \sin\phi - C_D \cos\phi) \xi^2 d\xi d\psi \tag{28}$$

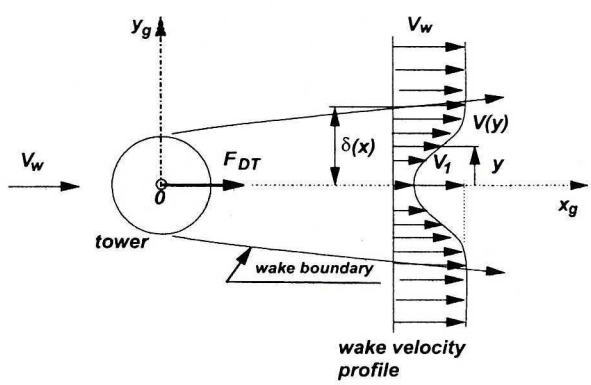

Fig. 4. The assumed tower wake model

For a typical rotor design, the angle α_r is small (less than 6°), and therefore the component of power given by (28) is negligible. Note that for non-yawed inflow condition the shaft power depends only on coefficient given by (29).

In the present work, the useful power is calculated from the formula:

$$P = \frac{\rho V_w^3 \pi R^2}{2}\left(C_{PM} - C_{Py}\right) \tag{29}$$

For the case of turbine with rotor placed behind the tower, a simple model of the tower shadow has been applied. The model is similar to that presented in [16] or [27], and is based on the momentum theorem. The assumed velocity distribution has been described by the following function:

$$\frac{V\left(x_g, y_g, z_g\right)}{V_w\left(z_g\right)} = 1 - \frac{V_1}{V_w\left(z_g\right)}\left(1 + \cos\pi \frac{y_g}{\delta_w\left(x_g/d_T\right)}\right) \tag{30}$$

where velocity deficit V_1 is given by formula:

$$\frac{V_1}{V_w\left(z_g\right)} = \frac{2}{3}\left(1 - \sqrt{1 - \frac{3}{2}\frac{d_T}{\delta\left(x_g\right)}C_{DT}}\right) \tag{31}$$

and the wake half-width δ_w is given by formula [19]:

$$\delta_w\left(x_g\right) = 0,9466 d_T \sqrt{C_{DT}\frac{x_g}{d_T}} \tag{32}$$

It was assumed that vertical wind profile is described by a logarithmic law:

$$\tilde{V}_w = \frac{V_w\left(z_g\right)}{V_w\left(H\right)} = \frac{\ln\left(z/z_0\right)}{\ln\left(H/z_0\right)} \tag{33}$$

Where z_0 is the effective height of terrain roughness.

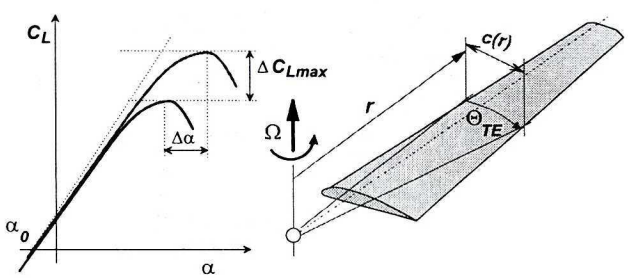

Fig. 5. Blade element stall delay. Schematic

In the present paper, two-dimensional rotor section characteristics have been corrected for stall-delay due to rotation. The correction was made by

the use of empirical stall delay model proposed by Tangler and Selig [23]. The angle of attack corresponding to the trailing edge separation α_n and the stall angle (critical angle of attack) α_s were increased by addition of stall delay angle $\Delta\alpha$ given by the formula:

$$\Delta\alpha = [(7,353K\Theta_{TE})^g - 1] \tag{34}$$

where:

$$K = 0,1754\,(c/r)^{-0,923} \tag{35}$$

The meaning of variables in formulae (35) and (36) is explained in Fig. 5.

The lowest suggested value of exponent g was 0,80 [23]. However, the lower value $g = 0,75$ gives a better fit for the power curve.

3. Comparison of the present model with experimental data

To compare the presented theory with experiment, 100 kW Risϕ three blade test turbine experimental data were chosen. One of the blades of the HAWT was instrumented to provide measurement of angles of attack, as well as forces acting on selected blade segments. There was a possibility to obtain long time series (up to 600 *sec.*) of the data, such as angle of attack at $r = 0.71R$, wind speed, rotor yaw angle, power output, rotor speed, and normal as well as tangential forces acting on three selected blade segments. The detailed description of the facility as well as experimental data one may find in [18]. However, for orientation, some of the main characteristics of the turbine are given in Table 3.1. The report [18] gives aerodynamic characteristics of the employed blade sections for a wide range of angles of attack (0°...90°). Mechanical and electrical power curves of the turbine are available, as well.

The calculations were conducted for the case of non-yawed and yawed conditions. The results were compared with experimental data obtained from the rotor field tests [18]

Fig. 6 shows mechanical power generated by a "constant-speed" ($n = 47,5rpm$) rotor for various wind velocities. The calculations have been made for several values of exponent g in stall-delay formula (35) The comparison of the predicted power output curve with the results obtained for tilted rotor shows a good agreement with experimental data. The best fit of power curve is obtained for $g = 0,75$. However, for low wind velocities, the present theory slightly underestimates power, but maximum power value is slightly overestimated. It is worth noticing that for low wind velocities there is no

Table 3.1.

Basic data of the Risφ 100 kW test facility [18]		
Hub height:	23,9	m
Rotor diameter:	19,0	
Blade length:	8,2	
Blade extensions:	1,0	
Root chord:	1,09	
Tip chord:	0,45	
Blade twist:	15	[deg]
Tilt angle:	5	
Cone angle:	0	
Rotor speeds (synchronous):	47,5 35,6	[rpm]
Airfoils:	NACA 63 2XX	
Power control:	stall	

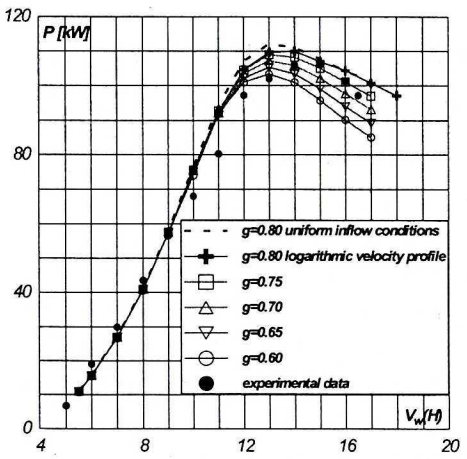

Fig. 6. Shaft power curve as a function of wind velocity for non-yawed rotor

significant difference between power calculated for rotor working in the logarithmic velocity profile and for rotor working in axial inflow. The appreciable difference appears only for high wind velocities (over 10 m/s), and does not depend on the value of g exponent.

The comparison of time-averaged angle of attack [18] measured by five hole Pitot tube at $r/R = 0,714$ with calculated values is presented in Fig. 7. The difference increases when tip speed ratio decreases. The values are slightly overestimated for small tip speed coefficients. For higher values of λ, the

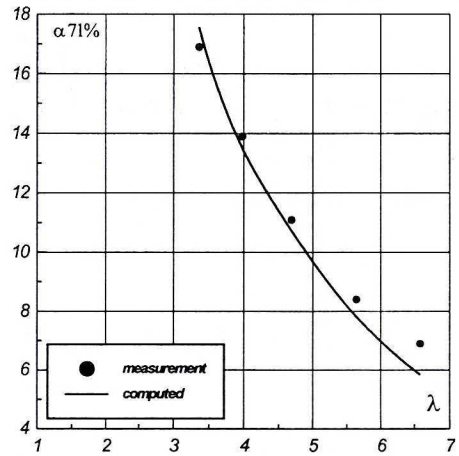

Fig. 7. Time-averaged angle of attack at r/R=0,71 vs. tip speed ratio

values are underestimated. This is in accordance with the differences between power curves presented in Fig. 6. The maximum difference, however, does not exceed one degree.

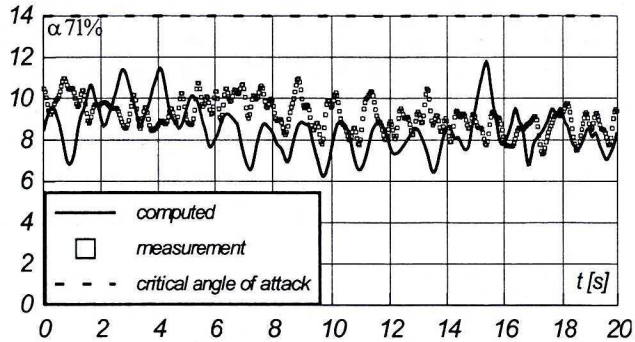

Fig. 8. Measured and calculated angle of attack time series V_w=8,4 m/s, λ=5,63

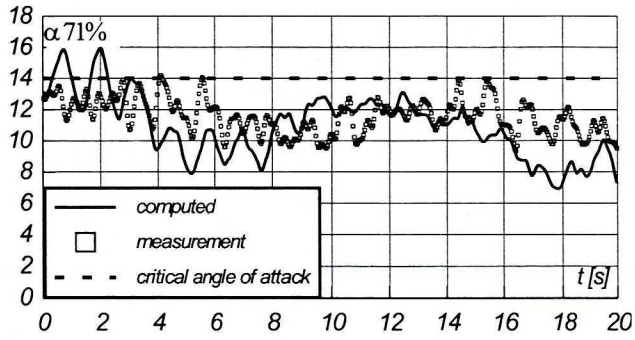

Fig. 9. Measured and calculated angle of attack time series V_w=10,1 m/s λ=4,68

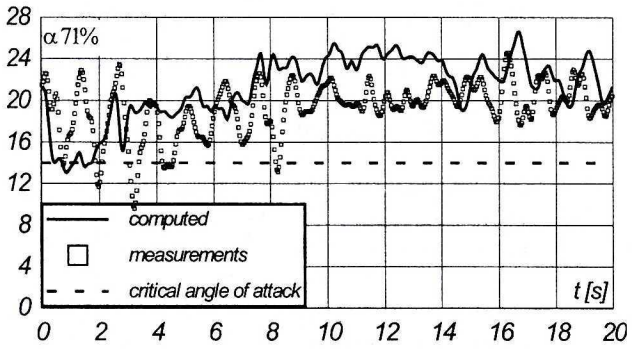

Fig. 10. Measured and calculated angle of attack time series V_w=14,1 m/s λ=3,35

The comparison of the calculated and measured time series of angle of attack is presented in Fig. 7...9. In this case, local angles of attack have bee calculated for time dependent wind speed and direction, measured at hub height [18]. The agreement between experimental data and computational results is good. The discrepancy between the computational results is mainly due to atmospheric turbulence and twist of wind direction.

The calculated power curves for yawed inflow condition are shown in Fig. 11. The available data from the field tests of the rotor are plotted as filled circles. The agreement between calculations and measurements is very good. The comparison of the numerical values from experiment and those from calculations is shown in Table 3.2. The maximum error is equal to 2,65%. The illustration of power loss due to the rotor side force Fy is shown in Fig. 12. The value of the power increases with wind speed and yaw angle.

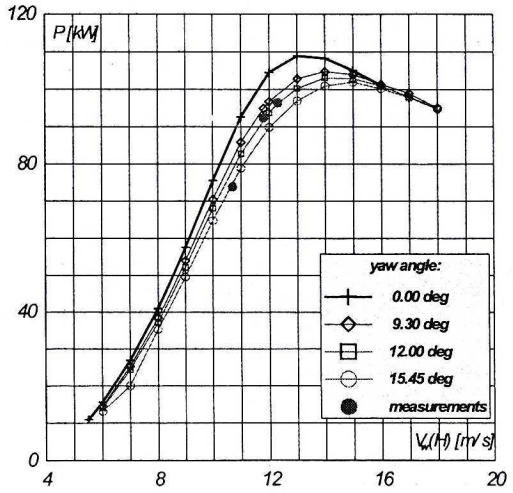

Fig. 11. Shaft power curve as a function of wind velocity for yawed rotor

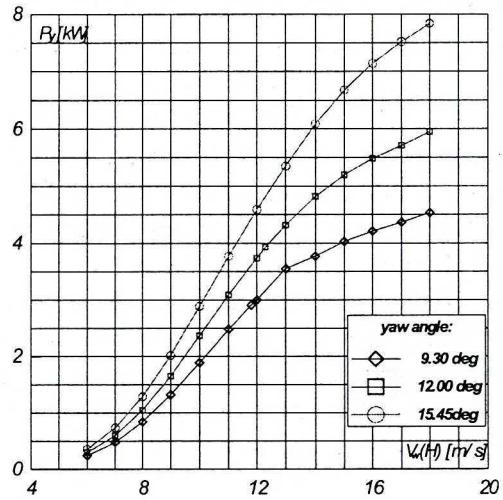

Fig. 12. The power loss related to the side force Fy at yawed flow condition

Table 3.2.

V_w m/s	ϕ_y [deg]	P [kW]			
		field tests [18] η_{gen}=0,894		Calculated	
		Electric power	Shaft power	Shaft power	Side force power
10,7	15,45	66,11	73,95	74,95	3,52
11,8	9,3	82,66	92,46	94,98	2,91
12,3	12,0	86,2	96,42	96,14	3,93

Table 3.3.

Basic data of the NREL 19,8 kW test facility [18]		
Hub height:	17,03	m
Rotor diameter:	10,06	
Blade length:	4,31	
Blade extensions:	0,724	
Root chord:	0,4572	
Tip chord:	0,4572	
Blade twist:	44,67	[deg]
Tilt angle:	0	
Cone angle:	3,42	
Rotor speeds (synchronous):	71,63	[rpm]
Airfoils:	NREL 809	
Power control:	stall	

The second comparison of experimental and computed data results concerns small, Grumman Wind Stream 33 turbine, modified by NREL [18] The three blade rotor is placed behind the tower relative to wind direction. The tower diameter is 0,4064 m The distance between tower and the blade axis is 1,32 m. Main geometric characteristics are collected n Table 3.3 The detailed description of the turbine one may find in [18].

Because of the altitude of test site, an air density of 0,9793 kg/m^3 has been chosen for calculations. The value is recommended by the authors of the report [18]. The efficiency of generator in these conditions is 78% The estimated value [18] of efficiency of transmission system was 98%. The drag coefficient for the tower sections was assumed to be equal to the drag coefficient of the cylinder of the same diameter. The numerical values of the C_{DT} as a function of Re was taken from [31].

Table 3.4.

V_w m/s	ϕ_y [deg]	P [kW]			
		field tests [18] η_{gen}=0,764		Calculated	
		Electric power	Shaft power	Shaft power	Side force power
6,1	-35,4	-3,20	-4,18	0,164	0,06
7,0	-18,5	-0,30	-0,393	2,410	0,15
7,8	21,4	0,50	0,66	3,39	0,25
8,2	39,4	-0,20	-0,26	1,72	0,27
8,8	24,2	3,40	4,45	4,69	0,42
10,2	-14,4	5,20	6,81	8,16	0,48
13,1	22,8	9,20	12,04	12,27	1,34
13,3	-19,0	9,90	12,96	13,52	1,23

The results of calculations for symmetrical inflow case are depicted in Fig. 13 whereas the data from yawed campaigns are collected in Table 3.4. and presented in Fig. 14. The results of computations for non-yawed conditions show good agreement as far as the slope power curve is concerned. However, the experimental curve is shifted left relative to the computational curve. This may be caused by lower than nominal (12 deg) blade setting angle due to the restoring moment resulting from centrifugal forces. The data for tests of yawed rotor show good correlation with the computational results for strong winds and relatively small yaw angles.

4. Final remarks and conclusions

The results presented above show good agreement with available experimental data for symmetrical and yawed inflow conditions. It was shown that

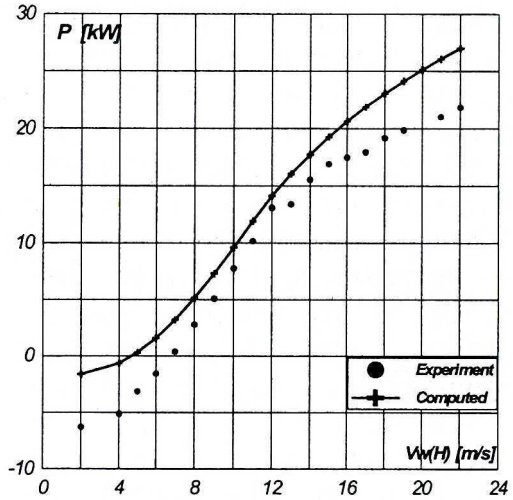

Fig. 13. Shaft power curve as a function of wind velocity for non-yawed rotor. Blade tip setting: 12 deg

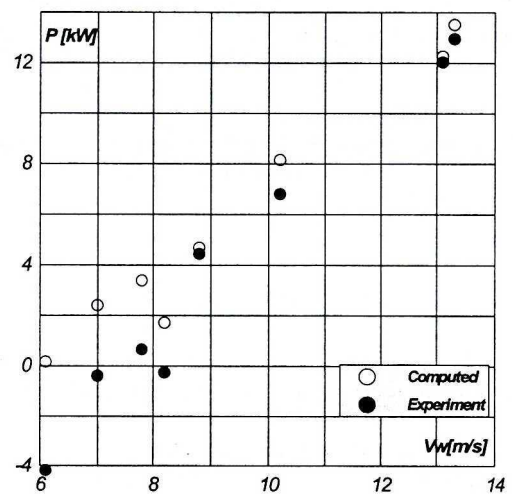

Fig. 14. Shaft power as a function of wind velocity for yawed rotor. Blade tip setting: 12 deg

for yawed inflow the power loss due to the work done by side force must be taken into account. Te differences between measured and calculated power curves are caused by applying a too simple model of stall delay. For the series of attack angle, one may observe time shift between calculations and experimental data. This may be due to the fact that five-hole Pitot probe, used for measurements, [18] was forwarding the blade in azimuth. The relationship (31) describes only an average wind profile, ignoring local turbulent fluctuations and twist of wind direction as a function of z coordinate. A quasi-steady model of aerodynamics (no dynamic stall) of blade element has

been employed in the present theory. The reason for this assumption was the fact that there were no indications allowing to separate effects caused by steady rotation generated stall delay from the dynamic stall. The above effects should have an influence on the time history of angle of incidence. In the presented study, however, it was assumed that time-averaged yaw angle is small, so there is no need to introduce any skewed wake corrections. This assumption ensued from particular conditions of experiment [18].

It was found that the present model of HAWT has a limitation ensued from physical conditions: for "constant-speed" HAWT the relative induced velocity ("induction factor") $a=(V_x - V_w)/V_w$ increases when wind velocity decreases. The calculations have shown that the model fails when, for any blade element, the induction factor reaches a value of about $a \approx 0{,}60$. Of course, the exact limiting value of a depends on geometry of the blade element. However, for the regime called "vortex ring state", such a simple theoretical model should not be applied.

As far as static aeroelasticity is concerned, the blade torsional stiffness distribution is unknown [18]. This knowledge could be useful to correct blade loading distribution for averaged inflow conditions, and improve performance estimations.

Manuscript received by Editorial Board, June 20, 2006;
final version, October 03, 2006.

REFERENCES

[1] Afijeh A. A., Keith T. G.: A simplified free wake method for horizontal-axis wid turbine performance prediction, transactions of the ASME. Journal of Fluid Engineering, 1986, No. 108. pp. 303÷309.

[2] Bareiß R.: The free wake/hybrid wake code ROVLM - a tool for aerodynamic analysis of wind turbines. Proceedings of ECWEC'93, Travemünde 1993.

[3] Askin V. E., Wild'grube L. S., Vozhdaev E. S., Majkapar G. I.: Lifting propeller theory. Maszinostrojenije, Moskwa 1973.

[4] Bermudez L, Velázquez A., Matesanz A.: Numerical simulation of unsteady aerodynamics effects in horizontal-axis wind turbines. Solar Energy, 2000, Vo. 68, No. 1, pp. 9÷21.

[5] Bussel van G. J. W.: The aerodynamics of horizontal axis wind turbine rotors explored with asymptotic expansion methods. TU Delft 1995.

[6] Bussel van G. J. W.: The use of asymptotic acceleration potential method for horizontal axis wind turbine rotor aerodynamics. J. of Wind Engineering and Industrial Aerodynamics, 1992, No. 38, pp. 161÷172.

[7] Dumitrescu H., Cardoş V.: Perdictions of unsteady HAWT aerodynamics by lifting line theory. Mathematical and Computer Modeling, 2001, No. 33, pp. 469÷481.

[8] Glauert H.: Elements of airfoil and airscrew theory. Cambridge University Press 1948.

[9] Hall G.: A method of analysis of propellers at extreme angles of attack. Journal of Aircraft, Jan.-Feb 1969, Vol 6, No. 1, pp. 52÷58.

[10] Huyer S. A., Simms D., Robinson M.C.: Unsteady aerodynamics associated with a horizontal-axis wind turbine. AIAA Journal, Vol. 34, No. 7 July 1996.
[11] Johnson W.: Helicopter Theory, Princeton University Press, 1980.
[12] Kotb M.A., Soliman H. A.: Performance of a horizontal-axis wind turbine under non-uniform flow with swirl. Journal of Wind Engineering and Industrial Aerodynamics, 1991, No. 37, pp.103÷111.
[13] Magnusson M. Near-Wake Behavior of Wind Turbines, Journal of Wind Engineering and Industrial Aerodynamics, 1999, No. 80, pp. 147÷1967.
[14] Manwell J.F., McGowan J.G., Rogers A.L.: Wind energy explained: theory design and application. John Wiley and Sons, New York 2002.
[15] Miller R. H. The aerodynamics and dynamic analysis of horizontal axis wind turbines. Journal of Wind Engineering and Industrial Aerodynamics, 1983, No. 15, pp. 329÷340.
[16] Moriarty P. J., Hansen A.C.: AeroDyn Theory Manual. NREL Technical Report NREL/TP-500-36881, January 2005.
[17] Politis G, K., Loukakis T. A.: On lifting line analysis of horizontal axis wind turbines. Wind Engineering, 1984, Vol. 8, No. 1, pp. 23÷35.
[18] Schepers J. G., et al.: Final Report of IEA ANNEX XIV: Field Rotor Aerodynamics, ECN-C-97-027, June 1997.
[19] Schlichting H.: Boundary layer theory. McGraw-Hill, New York 1981.
[20] Sorensen J. N., Kock C. W.: A model for unsteady rotor aerodynamics. Journal of Wind Engineering and Industrial Aerodynamics, 1995, No. 58, pp. 259÷275.
[21] Strzelczyk P.: Determination of horizontal axis wind turbine performance by use of simplified vortex theory. Transactions of the Institute of Aviation, 2/2000 (161), pp. 24÷33.
[22] Strzelczyk P.: Computational analysis of influence of blade geometry on performance of horizontal axis wind turbine. Transactions of The Rzeszów University of Technology, Nr 179/2000, pp. 383÷390, Proceedings of The International Scientific Conference "Mechanics 2000".
[23] Strzelczyk P.: Method of calculation of normal force on propeller at angle of attack by simplified vortex method. The Archive of Mechanical Engineering, 2004, Vol. LI, No. 4, pp. 515÷531.
[24] Sung Nam Jung, Tae-Soo No, Ki-Wahn Ryu: Aerodynamic performance prediction of a 30kW counter-rotating wind turbine system. Renewable Energy, 2005, No 30, pp. 631÷644.
[25] Tangler J. L., Selig M. S.: An evaluation of an empirical model for stall delay due to rotation for HAWTs, NREL/CP-440-23258, 1997.
[26] Vermeer N. J.: A review of wind turbine wake research at TU Delft AIAA paper. AIAA-2001-0030.
[27] Wang T., Coton F. N.: A high resolution tower shadow model for downwind turbines. Journal of Wind Engineering and Industrial Aerodynamics, 2001, No. 89, pp. 873÷892.
[28] Whale J., Anderson C. G., Bareiss R., Wagner S.: An experimental and numerical study of vortex structure in the wake of wind turbine. Journal of Wind Engineering and Industrial Aerodynamics, 2000, No. 84, pp. 1÷21.
[29] Witoszyński Cz.: "The Propeller" in: Selected papers. PWN Warszawa 1957, pp. 219÷245, (in Polish).
[30] Wilson R. E., Lissaman B. S.: Aerodynamic performance of wind turbines. NTIS Report PB-259-089. Oregon State University, Corvallis.
[31] Żurański J. A.: Obciążenie wiatrem budowli i konstrukcji. Arkady, Warszawa 1978 (in Polish).

Obliczanie charakterystyk turbiny wiatrowej o poziomej osi obrotu w warunkach napływu skośnego z wykorzystaniem uproszczonej teorii wirowej

Streszczenie

W artykule przedstawiono pewną metodę obliczania charakterystyk energetycznych turbiny wiatrowej w warunkach napływu skośnego. Przedstawiony model jest oparty na teorii śmigła przestawionej w pracy [23]. Model ten wykorzystuje wyniki wirowej teorii śmigła w połączeniu z zasadą pędu i momentu pędu dla strumienia zawirnikowego turbiny wiatrowej. W modelu tym element łopat traktowany jest jako źródło siły osiowej i siły stycznej działających na powietrze w płaszczyźnie kręgu roboczego wirnika. Równania wynikające z zasady pędu i momentu pędu zostały skorygowane ze względu na skończoną liczbę łopat wirnika poprzez wprowadzenie współczynnika Prandtla. Wprowadzenie aproksymacji siły nośnej za pomocą sinusoidy pozwoliło na otrzymanie równania kwadratowego ze względu na lokalną osiową prędkość przepływu w płaszczyźnie kręgu roboczego. Składowa obwodowa jest obliczana ze związków wynikających z uproszczonej teorii wirowej. Opisane rozwiązanie pozwala na uniknięcie iteracyjnego wyznaczania prędkości indukowanych.

W przeciwieństwie do większości metod obliczania osiągów śmigieł i turbin wiatrowych. Opór elementu łopaty jest uwzględniany w obliczeniach mocy i naporu na wirnik po wyznaczeniu prędkości indukowanych i kątów natarcia. W celu uwzględnienia opóźnienia oderwania na skutek oddziaływania siły Coriolisa na warstwę przyścienną zastosowano półempiryczny model Seliga-Tanglera. Prezentowany model zweryfikowano w oparciu dane eksperymentalne dla 100 kW turbiny doświadczalnej w Ris i seryjnej turbiny Grumman Wind Stream 33 zmodyfikowanej przez NREL.

Porównanie objęło zarówno krzywą mocy jak również zmierzone kąty natarcia. Uzyskane wyniki wykazują dobrą zgodność prezentowanego modelu z danymi doświadczalnymi. W artykule wskazano również na konieczność uwzględnienia mocy zależnej od siły bocznej w napływie skośnym, w celu otrzymania poprawnego przebiegu krzywej mocy.